arXiv:0806.2624v1 [physics.atom-ph] 16 Jun 2008

Low-energy molecular collisions in a permanent magnetic trap

Brian C. Sawyer, Benjamin K. Stuhl, Dajun Wang, Mark Yeo, and Jun Ye
JILA, National Institute of Standards and Technology and the University of Colorado
Department of Physics, University of Colorado, Boulder, Colorado 80309-0440, USA
(Dated: June 16, 2008)

Cold, neutral hydroxyl radicals are Stark decelerated and confined within a magnetic trap consisting of two permanent ring magnets. The OH molecules are trapped in the ro-vibrational ground state at a density of $\sim 10^6$ cm^{-3} and temperature of 70 mK. Collisions between the trapped OH sample and supersonic beams of atomic He and molecular D_2 are observed and absolute collision cross sections measured. The He–OH and D_2–OH center-of-mass collision energies are tuned from 60 cm^{-1} to 230 cm^{-1} and 145 cm^{-1} to 510 cm^{-1}, respectively, yielding evidence of reduced He–OH inelastic cross sections at energies below 84 cm^{-1}, the OH ground rotational level spacing.

PACS numbers: 34.50.-s, 34.50.Ez, 37.10.Mn, 37.10.Pq

Research in the field of cold polar molecules is progressing rapidly. An array of interesting topics is being developed, including precision measurement and fundamental tests [1, 2, 3], quantum phase transitions [4], and ultracold chemistry [5, 6]. In particular, dipolar molecules with well defined quantum states will enable us to exquisitely control their interactions via applied electric fields [7, 8]. The long-range, anisotropic interactions between dipolar molecules lead to new types of collision dynamics that could be used for novel collective effects [9, 10], quantum state engineering, and information processing.

Ultracold heteronuclear molecules have been produced via magnetic association or photoassociation of dual-species ultracold atom pairs [11, 12]. Most of these molecules are in excited rovibrational states, permitting ultracold atom–molecule collision studies to probe molecular decay processes [13, 14]. Coherent control techniques via exquisite manipulation of light fields are being developed to drive these internally excited molecules produced in the initial association step into deeply bound states with large dipole moments [15, 16]. High efficiencies expected in the optical transfer process will lead to unprecedented densities of ultracold polar molecules for studies of ultracold dipolar collisions and reactions.

Cold polar molecules in the ground state can be directly produced via cryogenic buffer gas cooling or Stark deceleration, but at temperatures typically in the range of 10 mK - 1 K. For example, buffer gas cooling methods have allowed for magnetic trapping of NH [17] and CaH [18] at ~ 1 K. The presence of the cooling He atoms naturally led to the studies of He - molecule collisions [19] and the observation of the quadratic dependence of the inelastic spin relaxation collision rate on rotational constant for $^3\Sigma$ NH molecules. Stark deceleration of supersonic molecular beams readily produces state-selected, ~ 100 mK samples at densities of 10^6–10^8 cm^{-3} [20, 21]. Stark decelerated molecules have been used in crossed-beam collisions with atomic species such as Xe [22].

In this Letter, we describe the confinement of cold dipolar molecules in a permanent magnetic trap loaded from a Stark decelerator. The open trap geometry facilitates low-energy molecule–molecule collision studies. We present total collision cross sections for D_2–OH and He–OH collisions within a magnet trap confining Stark-decelerated OH molecules. The atomic and molecular beams are produced in a supersonic nozzle cooled by liquid nitrogen, and the He–OH and D_2–OH center-of-mass collision energies can be tuned from 60 cm^{-1} to 230 cm^{-1} and 145 cm^{-1} to 510 cm^{-1}, respectively. Our magnetic trap design permits the application of electric dipole fields of tunable strength [23] that can be used to study novel dipolar collisions such as between fully polarized OH and NH_3. Both buffer-gas cooling [24] and Stark deceleration produce a large class of cold polar molecule beams. In combination with the trap described here, a wide variety of chemically interesting inter-species collisions can be studied at hitherto unexplored collision energies.

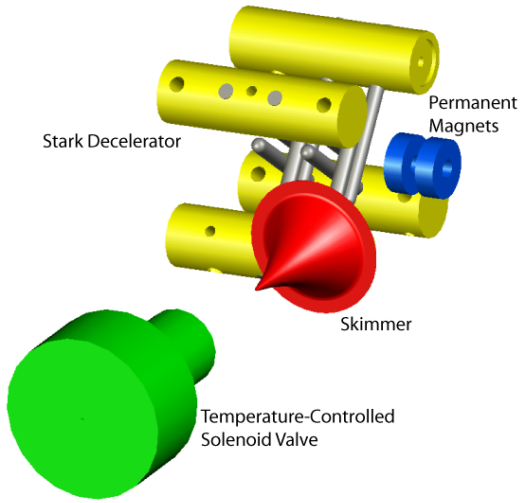

FIG. 1: (color online) Illustration of the magnetic trap and pulsed valve assemblies. The foreground contains the temperature-controlled solenoid valve and 1 mm diameter skimmer. The final stages of the Stark decelerator and permanent ring magnets of the trap are shown in the background.

Importantly, collisions between hydrogen (H, H_2) and

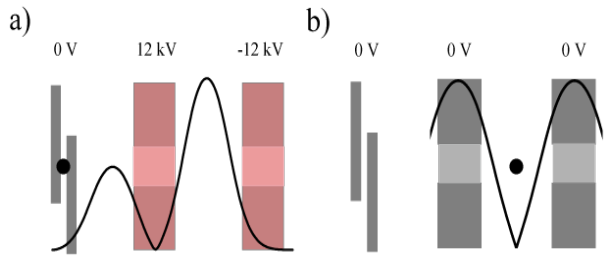

FIG. 2: (color online) Illustration of the trap loading sequence. (a) High voltage is applied to the surfaces of the two permanent ring magnets 1 μs after the final deceleration stage (shown at left) is grounded. The OH packet is stopped directly between the two magnets by the electric field gradient in 400 μs. The stopping potential due to the applied electric field is depicted. (b) The magnet surfaces are grounded, leaving the packet trapped within the displayed permanent magnetic quadrupole potential.

larger polar molecules (OH, H_2O, CO, H_2CO, SiO) are of astrophysical interest due to their possible role as pumps for interstellar masers [25]. In particular, specific emission lines of interstellar OH (1720 MHz) and H_2CO (4.8 GHz) masers have been attributed to collision-induced inversion by H_2 [26, 27]. By directly comparing D_2–OH cross sections with those of the more theoretically tractable He–OH, we will aid molecular collision theory at energy scales below 200 cm^{-1}.

A pulsed supersonic beam of OH radicals is produced by striking an electric discharge through a mixture of 27 mbar H_2O and 1.5 bar Kr. The resulting OH beam consists of rotationally cold, $^2\Pi_{3/2}$ molecules whose center longitudinal velocity is 490 m/s. The packet passes through a 3 mm diameter skimmer and is then coupled via an electrostatic hexapole into the 142-stage Stark decelerator. The Stark decelerator slows weak-field seeking OH molecules residing in the $|J = 3/2, m_J = \pm 3/2, f\rangle$ state, where J represents total angular momentum and m_J is the projection of J along the electric (E) field axis. The third quantum number denotes the parity of the state. The design and operating principle of this decelerator is discussed in previous work [21, 28]. The Stark decelerator is operated at a phase angle ϕ_0 of 50.352° in order to slow a 120 mK portion of the OH packet to 36 m/s. When slowing to velocities below 50 m/s, we observe maximum decelerator efficiency for $45° \leq \phi_0 \leq 55°$. Operation at these intermediate phase angles increases transverse packet confinement and reduces the coupling between transverse and longitudinal motion [29, 30].

We stop and confine the decelerated 36 m/s OH packet within a permanent magnetic trap whose center lies 1 cm from the final decelerator rod pair. This trap, depicted in Fig. 1, represents a marked improvement over our previous magneto-electrostatic trap in both design simplicity and ultimate trapping efficiency [23]. The magnetic trap is constructed by mounting two Ni-coated NdFeB permanent ring magnets in an opposing orientation such that a magnetic quadrupole field is produced between them. The N42SH rating of these magnets ensures an operating temperature of up to 150°C and a residual magnetization of 1.24 T. The inner and outer radii of the magnets measure 2 mm and 6 mm, respectively, while their thickness is 4 mm. The center-to-center magnet spacing of 7 mm in this magnetic trap yields a longitudinal magnetic (B) field gradient of 2 T/cm. This longitudinal separation matches the extent of the molecular packet entering the trap region from the Stark decelerator and therefore maximizes the trap density.

Figure 2 illustrates the trap loading sequence used with the magnetic trap of Fig. 1. In Fig. 2(a), the Ni coatings of the ring magnets are charged to ±12 kV precisely 1 μs after the final deceleration stage is grounded. At this point, the magnets become high-voltage electrodes and serve as a final Stark-slowing stage for the 36 m/s molecules. In addition to the large stopping potential between the magnets, there exists a smaller potential between the final decelerator rod pair and the first trap magnet. This barrier reflects the small number of molecules with longitudinal velocity less than 25 m/s. However, the barrier's transverse E-field gradient serves to confine the slow molecules as they enter the trap region. The OH packet is brought to rest directly between the magnets in 400 μs, at which point the high voltage is switched off. Those hydroxyl radicals occupying the weak-magnetic-field-seeking $|3/2, 3/2, f\rangle$ state (50% of the stopped molecules) are then confined within a magnetic quadrupole trap measuring $k_B \times 480$ mK deep in the longitudinal dimension, where k_B is Boltzmann's constant. The trap potential is shown in Fig. 2(b). We note that a permanent magnet was used to reflect a molecular beam [32].

Typical time-of-flight data and corresponding three-dimensional Monte Carlo simulation results are displayed in Fig. 3(a). Decelerated and trapped molecules are detected via laser-induced fluorescence (LIF). Lenses mounted in-vacuum allow for a fluorescence collection solid angle of ∼0.1 sr. In Fig. 3(a), the large peak at 400 μs is the stopped OH packet imaged at trap center. Transverse oscillation of the trapped packet is observed in both data and simulation over 2 ms. The number and density of trapped OH are measured to be $>10^3$ and $\sim 10^6$ cm^{-3}, respectively. A temperature of 70 mK is estimated from Monte Carlo simulation, also consistent with the molecular packet delivered by the Stark decelerator. Due to the large quadrupole B-field present in the trap, only a fraction of the OH sample is detected as the longitudinal 5 GHz Zeeman shift near each magnet is larger than our LIF laser linewidth. This effect is included in the trap density estimates. Figure 3(b) displays the observed trap lifetime of 432 ± 47 ms, limited by collisions with background gas. The trap chamber pressure of 7.5×10^{-9} Torr consists of equal parts H_2O and Kr. We note that this trap would be ideal for proposed multiple-loading schemes for molecules such as NH [31].

The open structure of the magnetic trap allows for low

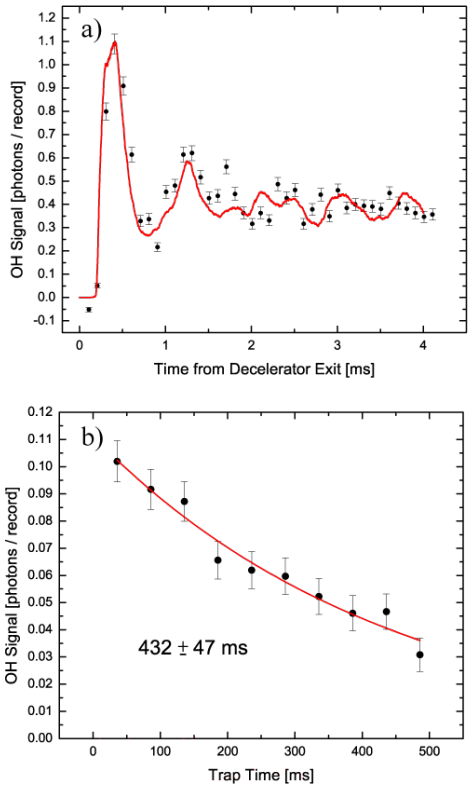

FIG. 3: (color online) (a) Time-of-flight data (circles with error bars) and three-dimensional Monte Carlo simulations (solid line) corresponding to OH trap loading. Stopping E-fields are switched off at 400 μs, which leaves 50% of the stopped OH molecules trapped in the permanent magnetic quadrupole. (b) Measurement of the lifetime of OH trapped within the magnetic trap at a background pressure of 7.5×10^{-9} Torr. A single-exponential fit (solid line) of the data yields 432 ± 47 ms.

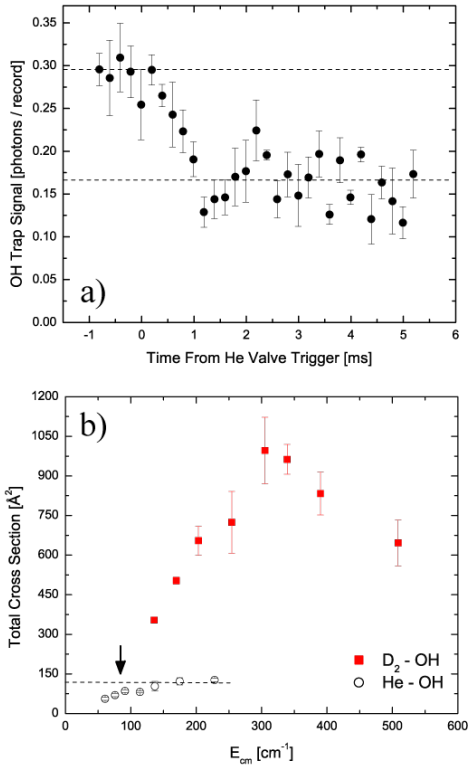

FIG. 4: (color online) (a) Time dependence of OH trap loss due to collisions with a supersonic He beam. Trap density drops sharply over 1 ms upon He beam collisions, then remains constant over the time scale shown. The valve is triggered 20 ms after the magnetic trap is loaded. (b) Total collision cross sections for He–OH (open circles) and D_2–OH (squares) as a function of E_{cm}. The decrease in the He–OH cross section at low energy is attributed to reduced inelastic loss as E_{cm} drops below the 84 cm^{-1} splitting between the $J = 3/2$ and $J = 5/2$ states of the OH molecule. The vertical arrow marks the 84 cm^{-1} point while the dashed line highlights this threshold behavior.

center-of-mass energy (E_{cm}) collision studies between the trapped OH and external molecular or atomic beams. As large electric fields are used only for initial trap loading, there is no risk of voltage breakdown when pulsing such beams through the trap. Furthermore, a relatively small polarizing E-field (few kV/cm) can be applied to the magnets after trap loading without loss of confined molecules—thereby enabling investigation of dipolar collisions. Figure 4 displays results from separately scattering beams of He and D_2 with the trapped OH sample. For this work, we place a pulsed solenoid valve (General Valve Series 99) and 1 mm diameter skimmer assembly, as shown in Fig. 1, such that the skimmed atomic or molecular beam passes directly between the magnets. The solenoid valve rests in a bath of liquid nitrogen while its 1 mm output nozzle is heated via 25 turns of manganin wire to allow for tuning of the beam velocity. All scattering data is taken at He and D_2 backing pressures of 2.0 and 2.7 bar, respectively. As expected, we observe that the beam velocities scale as the square-root of the nozzle temperature. The E_{cm} of the He–OH and D_2–OH systems can therefore be tuned to minima of ∼60 cm^{-1} and ∼145 cm^{-1}, respectively. Measurements of beam flux and velocity are made using a fast ionization gauge and a microphone-based pressure sensor placed 13 cm apart. The uncertainty in the inter-species calibration of the ionization gauge is ∼10%. The measured 8% velocity spread of the supersonic He beam gives a collision energy resolution of 9 cm^{-1} at the lowest nozzle temperature.

Figure 4(a) displays the time dependence of OH trap loss as a supersonic beam of He traverses the magnetic trap. Trap density drops sharply over the first ∼1 ms after the solenoid valve is fired, then remains constant over the time scale shown. Although the partial pressure of the scattering gas in the trap chamber rises as the supersonic beam scatters from the chamber walls, we measure an OH trap lifetime of >50 ms following the initial collision. Such vastly different time scales allow us to differentiate between trap loss due to the supersonic

beam and that resulting from background gas collisions. Trap loss at a given nozzle temperature is measured by repeatedly comparing OH population 1 ms *before* and 2 ms *after* the solenoid valve is triggered. The total cross sections of Fig. 4(b) are determined from the trap loss data by normalization to the corresponding beam flux measured with the fast ionization gauge at a given nozzle temperature. We also find that the trap loss scales linearly with the beam flux, confirming that we are operating in the single-collision regime.

An important advantage inherent to using trapped molecules as the scattering target is the ability to directly measure the absolute collision cross section. To do this, we use a leak valve to fill the trap chamber with a known pressure of He gas, then directly measure the OH trap lifetime at that pressure. The temperature of the chamber walls is 298 K, placing the E_{cm} of the thermal He–OH collisions at $\sim$250 cm^{-1}. The data point for He–OH collisions at 230 cm^{-1} from Fig. 4(b) is then scaled to this absolute cross section measuring 127 $\pm$ 18 Å^2.

For OH molecules in their ground electronic and vibrational state, the energy splitting of the two lowest lying rotational levels, $J = 3/2$ and $J = 5/2$, is 84 cm^{-1}. In a crossed-beam experiment, an abrupt decrease in the Xe–OH inelastic cross section was observed as E_{cm} was tuned below this value [22]. The He data of Fig. 4(b) possesses this feature. Because the magnetic trapping potential is sensitive to the internal state of the OH molecule, we cannot differentiate between trap loss due to elastic or inelastic collisions. Nevertheless, such a sudden decrease of the total cross section below 84 cm^{-1} is indicative of threshold behavior. The collision cross section of D_2–OH is larger than that of He–OH. This is understandable since the D_2 beam is an ortho/para mixture and contains a large fraction of frozen-in $J = 1$ population. The ratio of the two cross sections at 230 cm^{-1} is consistent with previous H_2–OH and He–OH pressure-broadening measurements made at a temperature of 298 K [33]. The enhanced collision cross sections for D_2–OH result from the quadrupole moment of the D_2 $J = 1$ state that can interact strongly at long range with the OH dipole. Yet another striking feature of the collision data is the pronounced peak in the D_2–OH cross section for $E_{cm} \sim 305$ cm^{-1}. Although more theoretical consideration is warranted, the 300 cm^{-1} $J = 3 \leftarrow J = 1$ transition of the $^1\Sigma_g^+$ D_2 molecule may be contributing to the inelastic cross section at this energy. Another possible explanation is collision-induced decay of $J = 2$ molecules present in an imperfect D_2 supersonic expansion.

In conclusion, we demonstrate a new permanent magnetic trap design that confines a dense sample of cold OH molecules as a cold collision target. Velocity-tunable supersonic beams of He and D_2 intersecting the magnetically trapped cold OH molecules yield absolute collision cross sections over an energy range of 60 cm^{-1} to 230 cm^{-1} and 145 cm^{-1} to 510 cm^{-1}, respectively. Threshold behavior is observed in He–OH collisions, and an enhancement of inelastic cross sections is seen in the D_2–OH system near 305 cm^{-1}. Having demonstrated the usefulness of this permanent magnetic trap for collision studies, future goals include using colder continuous beams of polar molecules as the colliding partner for OH. With the ability to apply a sufficiently strong polarizing field within the magnetic trap [34], we aim to reach sufficiently low E_{cm} to observe dipole-dipole interactions.

We acknowledge DOE, NSF, and NIST for funding support. We thank E. Meyer, J. L. Bohn, B. Lev, and J. M. Hutson for stimulating discussions and T. Keep and H. Green for technical assistance.

[1] J. J. Hudson et al., Phys. Rev. Lett. **89**, 023003 (2002).
[2] E. R. Hudson et al., Phys. Rev. Lett. **96**, 143004 (2006).
[3] B. L. Lev et al., Phys. Rev. A **74**, 061402(R) (2006).
[4] A. Micheli et al., Nature Physics **2**, 341 (2006).
[5] R. V. Krems, Intern. Rev. Phys. Chem. **24**, 99 (2005).
[6] E. R. Hudson et al., Phys. Rev. A **76**, 063404 (2006).
[7] L. Santos et al., Phys. Rev. Lett. **85**, 1791 (2000).
[8] A. V. Avdeenkov, D. C. E. Bortolotti, and J. L. Bohn, Phys. Rev. A **69**, 012710 (2004).
[9] K. Goral, L. Santos, and M. Lewenstein, Phys. Rev. Lett. **88**, 170406 (2002).
[10] S. Yi, L. You, and H. Pu, Phys. Rev. Lett. **93**, 040403 (2004).
[11] T. Kohler et al., Rev. Mod. Phys. **78**, 1311 (2006).
[12] K. M. Jones et al., Rev. Mod. Phys. **78**, 483 (2006).
[13] J. J. Zirbel et al., Phys. Rev. Lett. **100**, 143201 (2008).
[14] E. R. Hudson et al., Phys. Rev. Lett. **100**, 203201 (2008).
[15] J. Sage et al., Phys. Rev. Lett. **94**, 203001 (2005).
[16] S. Ospelkaus et al. (2008), arXiv/0802.1093; Nature Physics, in press.
[17] W. C. Campbell et al., Phys. Rev. Lett. **98**, 213001 (2007).
[18] J. Weinstein et al., Nature **395**, 148 (1998).
[19] W. C. Campbell et al. (2008), arXiv:0804.0265v1.
[20] H.L. Bethlem, G. Berden, and G. Meijer, Phys. Rev. Lett. **83**, 1558 (1999).
[21] J. Bochinski et al., Phys. Rev. Lett. **91**, 243001 (2003).
[22] J. J. Gilijamse et al., Science **313**, 1617 (2006).
[23] B. C. Sawyer et al., Phys. Rev. Lett. **98**, 253002 (2007).
[24] D. Patterson and J. M. Doyle, J. Chem. Phys. **126**, 154307 (2007).
[25] M. Elitzur, Rev. Mod. Phys. **54**, 1225 (1982).
[26] J. Guibert et al., Astron. Astrophys. **62**, 305 (1978).
[27] I. M. Hoffman et al., Astrophys. J. **598**, 1061 (2003).
[28] J. Bochinski et al., Phys. Rev. A **70**, 043410 (2004).
[29] S. Y. T. van de Meerakker et al., Phys. Rev. A **73**, 023401 (2006).
[30] B. C. Sawyer et al., Eur. Phys. J. D **48**, 197 (2008).
[31] S. Y. T. van de Meerakker et al., Phys. Rev. A **64**, 041401(R) (2001).
[32] M. Metsala et al., arXiv:0802.2902 (2008).
[33] K. Park et al., J. Quant. Spectrosc. Radiat. Transfer **55**,

285 (1995).
[34] R. V. Krems, Phys. Rev. Lett. **96**, 123202 (2006).